Catalysis Communications 90 (2017) 35–38

Contents lists available at ScienceDirect

Catalysis Communications

journal homepage: www.elsevier.com/locate/catcom

Short communication

Catalytic hydrogenation of 2-nitro-2′-hydroxy-5′-methylazobenzene over solid base-hydrogenation bifunctional catalysts: Effect of alkali metals on Pd/γ-Al_2O_3

Leilei Si, Bowei Wang, Shipeng Chen, Jingru Hou, Xilong Yan, Yang Li *, Ligong Chen

School of Chemical Engineering and Technology, Tianjin University, Tianjin 300350, PR China
Collaborative Innovation Center of Chemical Science and Engineering (Tianjin), Tianjin 300072, PR China

ARTICLE INFO

Article history:
Received 1 August 2016
Received in revised form 8 November 2016
Accepted 10 November 2016
Available online 11 November 2016

Keywords:
Benzotriazole
Catalytic hydrogenation
Palladium catalyst
Alkali metal

ABSTRACT

Alkali metals doped Pd solid base-hydrogenation bifunctional catalysts were prepared, characterized, and employed in the hydrogenation of 2-nitro-2′-hydroxy-5′-methylazobenzene. The results indicated that the basicity of catalyst endowed by the alkali metals indeed hindered the formation of amino by-products. Among them, K doped catalyst exhibited the best catalytic performance and 84.79% benzotriazole selectivity was obtained. Furthermore, besides the good distribution of palladium particles, it is important for basic sites to distribute around the palladium particles strictly, which is the guarantee of high benzotriazole selectivity.

1. Introduction

2-(2′-Hydroxy-5′-methylphenyl) benzotriazole (BTA) is one of the most important ultraviolet absorbers in industry, which is widely used for the protection of plastics against sunlight [1,2]. Currently, the major preparation methods of BTA are the catalytic reduction of 2-nitro-2′-hydroxy-5′-methylazobenzene (NAB) with reducing agents [3–9]. Although good yield of BTA is achieved, the serious pollution is still a big challenge [10]. In our previous work, we have successfully established a continuous synthetic technology of BTA, which is not only a green method but also an efficient process [11]. In addition, solid base-hydrogenation bifunctional catalysts have been also successfully employed in this reaction to avoid using additional base and then solve environmental problems caused by the use of extra lye [11,12]. It led to an entirely new line of BTA synthesis to use these kinds of bifunctional catalysts. Meanwhile, alkali metals doped Pd catalysts have always been one of the hot research topics [13,14]. However, this significant research is just getting started. There is still room for study and improvement.

In this work, further research on solid base-hydrogenation bifunctional catalysts was carried out to explore the effect of different alkali metals on Pd/γ-Al_2O_3. Although our previous work has confirmed that K doped Pd catalysts can efficiently hinder the formation of amino by-products, the understanding of structure-activity relationship is still insufficient. So we attempted to find the key factor of these solid base-hydrogenation bifunctional catalysts by doping different kind of alkali metals on Pd/γ-Al_2O_3. Does different kind of alkali metals produce the same or similar impact on Pd/γ-Al_2O_3? What is the relationship between basic amount of these bifunctional catalysts and their catalytic abilities? What is the key factor in the catalytic hydrogenation of NAB to BTA over alkali metals doped palladium bifunctional catalysts? In order to answer these questions, alkali metals (Na, K, Rb, Cs) doped Pd/γ-Al_2O_3 were prepared and their catalytic performances were evaluated. Moreover, these catalysts were characterized by Fourier transform infrared spectroscopy (FT-IR), X-ray diffraction (XRD), Brunauer-Emmer-Teller (BET) surface area measurement, temperature programmed desorption of carbon dioxide (CO_2-TPD), transmission electron microscopy (TEM), and elemental mapping and temperature programmed desorption of ammonia (NH_3-TPD) to investigate the structure-activity relationship.

2. Experimental

2.1. Preparation of catalysts

Pd/γ-Al_2O_3 was prepared by the method involved in our previous work [12]. The detailed process was put into the supplementary material, and Pd/γ-Al_2O_3 doped by $NaNO_3$ was named after Pd/γ-Al_2O_3-$NaNO_3$. The rest catalysts were named by same method.

---

* Corresponding author at: School of Chemical Engineering and Technology, Tianjin University, Tianjin 300350, PR China.
E-mail addresses: liyang777@tju.edu.cn (Y. Li), lgchen@tju.edu.cn (L. Chen).

http://dx.doi.org/10.1016/j.catcom.2016.11.015

2.2. Experimental procedure

The catalytic hydrogenation reaction was accomplished in a fixed-bed reactor with an inner diameter of 15 mm and a length of 650 mm, which was filled up with 40 mL catalysts with diameter of 3 mm and height of 3 mm averagely. The solution of NAB in toluene (the concentration of NAB is 5 wt%) was dosed into the reactor by the tranquil flow pump. The hydrogenation reaction was proceeding at temperature 60 °C, H_2 pressure 2.5 MPa, liquid hourly space velocity (LHSV) 0.23 h^{-1}. The samples for analysis were collected continuously and the frequency was once an hour. The composition of the reaction mixture was analyzed by high performance liquid chromatography (HPLC) with a column of Extend C_{18} (250 mm × 4.6 mm, 10 μm, Agilent technologies, USA).

3. Results and discussion

3.1. FT-IR

The FT-IR spectra of γ-Al_2O_3, Pd/γ-Al_2O_3, Pd/γ-Al_2O_3-$NaNO_3$, Pd/γ-Al_2O_3-KNO_3, Pd/γ-Al_2O_3-$RbNO_3$ and Pd/γ-Al_2O_3-$CsNO_3$ are shown in Fig. 1. As shown in Fig. 1, the peaks at 3450 cm^{-1} and 1632 cm^{-1} were caused by the O—H stretching and bending vibration of adsorbed water [12,15,16]. Compared with curves of γ-Al_2O_3 and Pd/γ-Al_2O_3, there were two new peaks at 1561 cm^{-1} and 1401 cm^{-1} in the spectra of curves of Pd/γ-Al_2O_3-$NaNO_3$, Pd/γ-Al_2O_3-KNO_3 and Pd/γ-Al_2O_3-$RbNO_3$. The two bands were attributed to CO_3^{2-} ions weakly bounded with M^+ (M = Na, K, Rb) present on the surface of the catalyst. The CO_3^{2-} ions might come from $K_2O \cdot CO_2$ species, which formed in the catalyst calcination [12,16–19]. However, intensity of the two absorption bands both weakened from curves of Pd/γ-Al_2O_3-$NaNO_3$ to Pd/γ-Al_2O_3-$RbNO_3$ in sequence. The result was partly caused by which $RbNO_3$ was only partly decomposed into Rb_9O_2 [20]. The spectra of curves of Pd/γ-Al_2O_3-$CsNO_3$ did not display the two peaks because $CsNO_3$ loading in the Al_2O_3 did not decompose at 500 °C [21]. The bands at 1113 cm^{-1} and 785 cm^{-1} in the all catalysts were caused by AlO_4 groups, and the bands at 581 cm^{-1} arose from AlO_6 groups. These results indicated the presence of Al-O-Al framework [12,22–24]. The shoulders at 1113 cm^{-1} and 785 cm^{-1} decreased gradually from curves of γ-Al_2O_3 to curves of Pd/γ-Al_2O_3-$CsNO_3$ and shifted to a sharp wavelength due to the effect of M^+ (M = Na, K, Rb, Cs) on the Al—O bonds (AlO_4 groups) [22,25]. This phenomenon also proved the all nitrates successfully load in the supports.

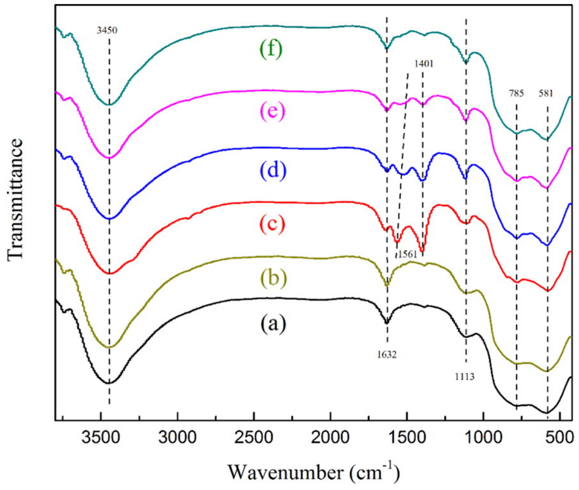

Fig. 1. FT-IR spectra. (a) γ-Al_2O_3; (b) Pd/γ-Al_2O_3; (c) Pd/γ-Al_2O_3-$NaNO_3$; (d) Pd/γ-Al_2O_3-KNO_3; (e) Pd/γ-Al_2O_3-$RbNO_3$; (f) Pd/γ-Al_2O_3-$CsNO_3$.

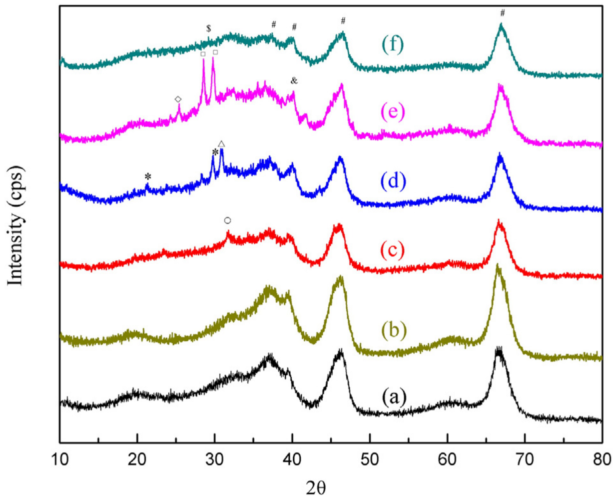

Fig. 2. X-ray powder diffractograms of (a) γ-Al_2O_3, (b) Pd/γ-Al_2O_3, (c) Pd/γ-Al_2O_3-$NaNO_3$, (d) Pd/γ-Al_2O_3-KNO_3, (e) Pd/γ-Al_2O_3-$RbNO_3$ and (f) Pd/γ-Al_2O_3-$CsNO_3$. (○), Na_2O; (*) Al-O-K; (△) K_2O; (◇) Rb_9O_2; (□) $RbNO_3$; ($) $CsNO_3$; (&) Pd (111); (#) γ-Al_2O_3.

3.2. XRD

The X-ray powder diffractograms of γ-Al_2O_3, Pd/γ-Al_2O_3, Pd/γ-Al_2O_3-$NaNO_3$, Pd/γ-Al_2O_3-KNO_3, Pd/γ-Al_2O_3-$RbNO_3$ and Pd/γ-Al_2O_3-$CsNO_3$ are shown in Fig. 2. The typical diffraction peaks at 2θ value of 37°, 46°, and 67° were attributed to γ-Al_2O_3 in all catalysts [11,12,26–28] (JCPDS 23-1009). The peaks at 2θ value of 40° in all curves cannot categorically be attributed to the (111) plane of face-centered cubic structure of Pd because the peaks of Al_2O_3 phases existed in the same position and the intensity of Pd diffraction peak was too weak due to the low loading [12,24,26,29]. Compared with Pd/γ-Al_2O_3, the three peaks of Al_2O_3 in other catalysts were relatively weak, which indicated that the interaction between alkali metals and Al_2O_3 affects the crystal of Al_2O_3. The peak at 2θ value of 32° in the curve of Pd/γ-Al_2O_3-$NaNO_3$ was ascribed to Na_2O phases (JCPDS 23-0528). The peaks at 2θ value of 21° and 29° in the pattern of Pd/γ-Al_2O_3-KNO_3 were attributed to orthorhombic α-$KAlO_2$ species formed on the catalyst surface [12,16,30]. The peaks at 2θ value of 31° were clearly observed in the curve of the Pd/γ-Al_2O_3-KNO_3 catalyst, which were ascribed to the K_2O species [12,19,25,31]. The peaks at 2θ value of 25° in the curve of the Pd/γ-Al_2O_3-$RbNO_3$ catalyst may be attributed to the Rb_9O_2 groups (JCPDS 28-0935). The peaks at 2θ value of 28° and 30° in the curve of the Pd/γ-

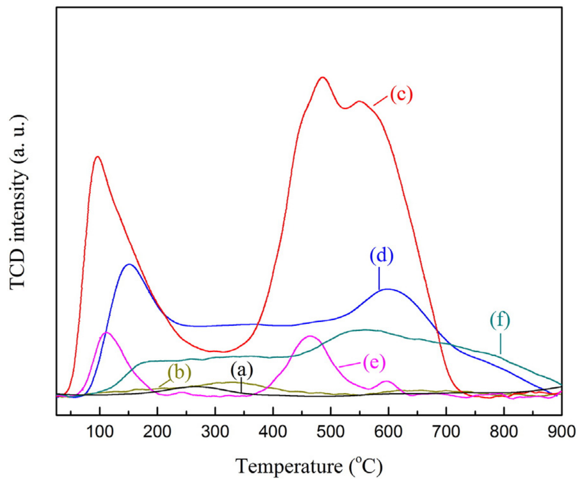

Fig. 3. CO_2-TPD curves of (a) γ-Al_2O_3, (b) Pd/γ-Al_2O_3, (c) Pd/γ-Al_2O_3-$NaNO_3$, (d) Pd/γ-Al_2O_3-KNO_3, (e) Pd/γ-Al_2O_3-$RbNO_3$ and (f) Pd/γ-Al_2O_3-$CsNO_3$.

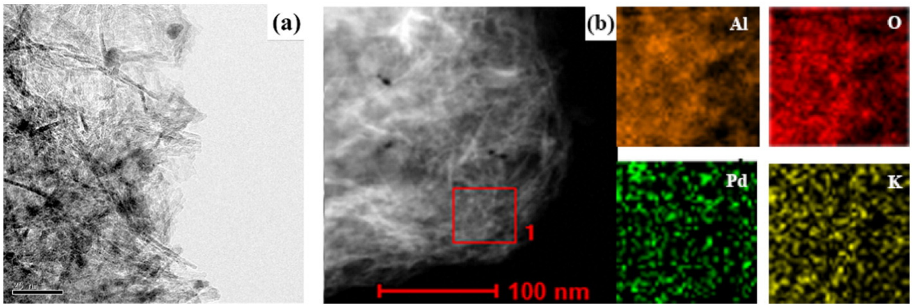

Fig. 4. TEM image of (a) Pd/γ-Al_2O_3-KNO_3 and elemental mapping of (b) Pd/γ-Al_2O_3-KNO_3.

Al_2O_3-$RbNO_3$ catalyst were ascribed to the $RbNO_3$ phases [20] (JCPDS 78-0112). These results were compliance with that the $RbNO_3$ did not completely decompose at 500 °C [20]. The peak at 2θ value of 29° in the curve of the Pd/γ-Al_2O_3-$CsNO_3$ catalyst were attributed to $CsNO_3$ phases (JCPDS 32-0252), indicating that the $CsNO_3$ did not decompose at 500 °C [21]. The peak was weak because the content of $CsNO_3$ was too low. The results were consistent with the FT-IR results.

3.3. CO_2-TPD

The CO_2-TPD profiles of γ-Al_2O_3, Pd/γ-Al_2O_3, Pd/γ-Al_2O_3-$NaNO_3$, Pd/γ-Al_2O_3-KNO_3, Pd/γ-Al_2O_3-$RbNO_3$, Pd/γ-Al_2O_3-$CsNO_3$ are presented in Fig. 3, which were employed to probe the alkaline information of all catalysts. From Fig. 3, the CO_2-TPD signal of Pd/γ-Al_2O_3 was rather weak due to its acidic nature [12,32], however, all alkali metals doped catalysts displayed remarkable and broad desorption peaks, indicating the presence of basic sites on the surface of Pd catalysts. Our previous work has demonstrated that the basicity of catalysts endowed by modification with alkali metals can effectively prevent the formation of by-products AC [12], which was further confirmed by this work. Among all bifunctional catalysts, Pd/γ-Al_2O_3-$NaNO_3$ exhibited the highest basicity amount, most probably because more Na atoms could support on Pd/γ-Al_2O_3 under the same mass loading, compared with K, Rb, and Cs. Moreover, the profile of Pd/γ-Al_2O_3-$CsNO_3$ was completely different from other catalysts, because $CsNO_3$ cannot decompose at 500 °C [21]. The above analyses were consistent with FT-IR and XRD results. Hence, in order to further understand the structure-activity relationship, TEM and elemental mapping were carried out.

3.4. TEM

TEM image and elemental mapping of Pd/γ-Al_2O_3-KNO_3 are shown in Fig. 4. It could be found that palladium particles were present as black dots on these bifunctional catalysts (Figs. 4a and S2a, c, e) [11,12,33]. Among them, the palladium particles on Pd/γ-Al_2O_3-$CsNO_3$ appeared serious agglomeration, which was further confirmed by elemental mapping (Fig. S2f). As everyone knows, the agglomeration of palladium particles tremendously restricts the catalytic activity [34]. Therefore, the performance of Pd/γ-Al_2O_3-$CsNO_3$ in the catalytic hydrogenation of NAB to BTA was awful. Meanwhile, it was noteworthy that palladium particles also partly aggregated on Pd/γ-Al_2O_3-$RbNO_3$ catalyst (Fig. S2c, d). Nevertheless, the distributions of palladium particles on Pd/γ-Al_2O_3-KNO_3 and Pd/γ-Al_2O_3-$NaNO_3$ were much better than those on Pd/γ-Al_2O_3-$RbNO_3$ and Pd/γ-Al_2O_3-$CsNO_3$. From Fig. S2b, it was obvious that sodium element evenly distributed on the support, however the sodium particles did not strictly distribute around the palladium particles. In the case of Pd/γ-Al_2O_3-KNO_3 sample, the distribution of potassium elements was similar with that of palladium particles [12], demonstrating that the basic sites were strictly dispersed around the active sites of hydrogenation.

3.5. Catalytic performance

Pd/γ-Al_2O_3, Pd/γ-Al_2O_3-$NaNO_3$, Pd/γ-Al_2O_3-KNO_3, Pd/γ-Al_2O_3-$RbNO_3$ and Pd/γ-Al_2O_3-$CsNO_3$ were employed for the catalytic hydrogenation of NAB to BTA without additional base in order to evaluate their catalytic performance. As shown in Table 1, 2-amino-*p*-cresol, *o*-phenylenediamine (AC) [35], 2-(2′-hydroxy-5′-methylphenyl)benzotriazole *N*-oxide (NO) and tetrahydro-2-(2′-hydroxy-5′-methylphenyl)benzotriazole (THB) together with BTA were all detected in the reaction mixture, which was confirmed by our previous work (Scheme 1) [11,12]. As expected, the conversion of NAB was satisfactory (>92%) over all catalysts, and the selectivity of by-products AC over Pd/γ-Al_2O_3-MNO_3 (M = Na, K, Rb, Cs) catalysts decreased sharply compared with Pd/γ-Al_2O_3, indicating the importance of alkaline environment to this reaction [11,12,35]. Among them, the AC selectivity over Pd/γ-Al_2O_3-KNO_3 was only 4.78% which is the lowest. For the selectivity of BTA, another important evaluation criterion, these four catalysts presented distinct catalytic performance. When Pd/γ-Al_2O_3-$NaNO_3$, Pd/γ-Al_2O_3-$RbNO_3$, and Pd/γ-Al_2O_3-$CsNO_3$ were used for this reaction, the selectivity of BTA were 30.11%, 36.05% and 19.59%, respectively, which were lower than that of Pd/γ-Al_2O_3. However, 84.79% selectivity of BTA was obtained with Pd/γ-Al_2O_3-KNO_3 as the catalyst. Meanwhile, compared with Pd/γ-Al_2O_3-KNO_3, even with Pd/γ-Al_2O_3, >17% THB selectivity and 21% NO selectivity were provided over Pd/γ-Al_2O_3-$NaNO_3$, Pd/γ-Al_2O_3-$RbNO_3$, and Pd/γ-Al_2O_3-$CsNO_3$. Nevertheless, the NO selectivity and THB selectivity over Pd/γ-Al_2O_3-KNO_3 were only 6.54% and 0.59%, respectively. Obviously, Pd/γ-Al_2O_3-KNO_3 exhibited the best

Table 1
Catalytic hydrogenation of NAB over catalysts.

Catalyst	Conversion (%)[b]	Selectivity (%)				
		AC	NO	BTA	THB	Others[c]
Pd/γ-Al_2O_3[a]	100.00 ± 0.00	25.39 ± 0.38	9.64 ± 0.63	59.08 ± 0.55	1.08 ± 0.11	4.81 ± 0.36
Pd/γ-Al_2O_3-$NaNO_3$[a]	92.49 ± 0.43	19.21 ± 0.19	21.16 ± 0.33	30.11 ± 0.85	19.34 ± 0.51	10.18 ± 0.62
Pd/γ-Al_2O_3-KNO_3[a] [12]	100.00 ± 0.00	4.78 ± 0.19	6.54 ± 0.25	84.79 ± 0.49	0.59 ± 0.06	3.30 ± 0.44
Pd/γ-Al_2O_3-$RbNO_3$[a]	99.89 ± 0.10	12.72 ± 0.69	29.06 ± 0.50	36.05 ± 0.63	17.89 ± 0.65	4.28 ± 0.13
Pd/γ-Al_2O_3-$CsNO_3$[a]	99.88 ± 0.17	16.80 ± 0.38	22.58 ± 0.54	19.59 ± 0.52	37.03 ± 0.40	4.00 ± 0.35

[a] Reaction conditions: temperature: 60 °C; hydrogen pressure: 2.5 MPa; liquid hourly space velocity (LHSV): 0.23 h^{-1}. Each data point is an average of three or more runs.
[b] The conversion of NAB.
[c] Including contamination in raw material, errors of measurement instrument and trace impurities produced in the reaction.

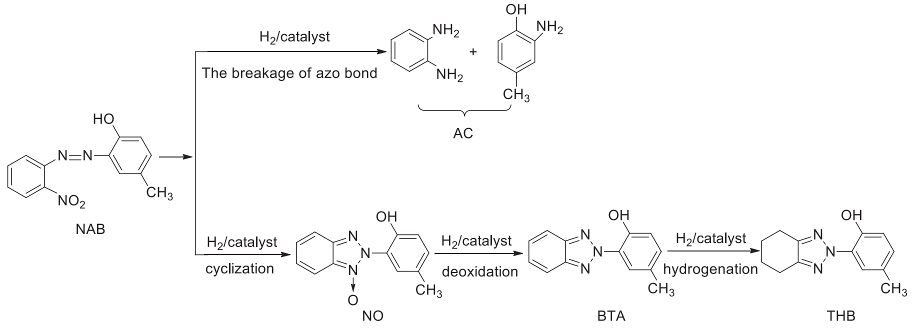

Scheme 1. Catalytic hydrogenation of NAB.

catalytic performance on the catalytic hydrogenation of NAB to BTA. Furthermore, it was found that no notable deactivation of Pd/γ-Al_2O_3-KNO_3 in activity was observed in 100 h (Fig. S1) [12].

Furthermore, it was interesting that the doping elements of the same group influenced the catalytic performance of Pd/γ-Al_2O_3 diversely. According to Fig. 3 and Table 1, it was easy to find that the mild strength basicity produced by Pd/γ-Al_2O_3-KNO_3 is important for the reaction. Combined with the TEM and the results of Table 1, the selectivity of BTA over Pd/γ-Al_2O_3-KNO_3 was much better than that over Pd/γ-Al_2O_3-$NaNO_3$ in the catalytic hydrogenation of NAB to BTA. So the distribution of basic sites was important for this reaction.

Therefore, it can be speculated that there are two key factors in the catalytic hydrogenation of NAB to BTA over alkali metals doped palladium bifunctional catalysts without additional base. One is the distribution of palladium particles. The other one is the dispersion of basic sites that must strictly distribute around the active sites of hydrogenation. Only then can the active sites of hydrogenation and basic sites synergistically catalyze NAB to BTA in high selectivity.

4. Conclusions

In summary, Pd/γ-Al_2O_3 catalysts modified by alkali metals (Na, K, Rb, Cs) were prepared and employed in the catalytic hydrogenation of NAB to BTA. The results indicated that Pd/γ-Al_2O_3-KNO_3 exhibited the best catalytic performance among these bifunctional catalysts and 84.79% BTA selectivity was obtained.

All catalysts were further characterized by FT-IR, XRD, BET, CO_2-TPD, TEM, elemental mapping and NH_3-TPD. The results of FT-IR and XRD indicated that Pd/γ-Al_2O_3 catalysts were successfully doped by alkali metals. The profiles of CO_2-TPD demonstrated that the basicity of catalyst endowed by modification with alkali metals can effectively hinder the formation of by-products AC. And the mild strength basicity produced by Pd/γ-Al_2O_3-KNO_3 is important for the reaction. Moreover, the characterizations of TEM and elemental mapping revealed that there are two key factors in the above mentioned reaction. One is the distribution of palladium particles, and the other is the dispersion of basic sites that must strictly distribute around the active sites of hydrogenation.

Acknowledgements

Financial support by the National Natural Science Foundation of China (Grant No. 21476163) are gratefully acknowledged.

Appendix A. Supplementary data

Supplementary data to this article can be found online at doi:10.1016/j.catcom.2016.11.015.

References

[1] J.C. Crawford, Prog. Polym. Sci. 24 (1999) 7–43.
[2] J. Catalán, M.R. Torres, J.D. Tornero, J. Chem. Soc. Faraday Trans. 93 (1997) 1691–1696.
[3] B.M. Francis, US Patent 3018269.
[4] R.J. Boyle, US Patent 3230194.
[5] A.S. ALzaydien, J. Appl. Sci. 4 (2004) 136–139.
[6] L. C. Vishwakarma, US Patent 5675015.
[7] S. Tanimoto, T. Kamano, Synthesis 1986 (1986) 647–649.
[8] H.L. White, US Patent 4041044.
[9] J. Rody, A.C. Rochat, US Patent 4001266.
[10] B.H. Kim, S.K. Kim, Y.S. Lee, Y.M. Jun, W. Baik, B.M. Lee, Tetrahedron Lett. 38 (1997) 8303–8306.
[11] B. Wang, W. Fang, L. Si, Y. Li, X. Yan, L. Chen, S. Wang, ACS Sustain. Chem. Eng. 3 (2015) 1890–1896.
[12] B. Wang, L. Si, Y. Yuan, Y. Li, L. Chen, X. Yan, RSC Adv. 6 (2016) 16766–16771.
[13] V. Vishwanathan, V. Jayasri, P.M. Basha, N. Mahata, L. Sikhwivhilu, N.J. Coville, Catal. Commun. 9 (2008) 453–458.
[14] W. Kim, Appl. Catal. A-Gel. 268 (2004) 77–82.
[15] W. Xie, H. Peng, L. Chen, Appl. Catal. A-Gel. 300 (2006) 67–74.
[16] X. Li, D. Yu, W. Zhang, Z. Li, X. Zhang, H. Huang, Appl. Catal. A-Gel. 455 (2013) 1–7.
[17] C. Murugan, H. Bajaj, R. Jasra, Catal. Lett. 137 (2010) 224–231.
[18] Y. Amenomiya, J. Catal. 55 (1978) 205–212.
[19] W. Xie, H. Li, J. Mol. Catal. A Chem. 255 (2006) 1–9.
[20] N. Uvarov, P. Vaněk, Y.I. Yuzyuk, V. Železný, V. Studnička, B. Bokhonov, V. Dulepov, J. Petzelt, Solid State Ionics 90 (1996) 201–207.
[21] P. Campbell, M. Ortner, C. Anderson, Anal. Chem. 33 (1961) 58–61.
[22] L. Fernández-Carrasco, E. Vázquez, Fuel 88 (2009) 1533–1538.
[23] Y. Ono, J. Catal. 216 (2003) 406–415.
[24] S. Hinokuma, K. Murakami, K. Uemura, M. Matsuda, K. Ikeue, N. Tsukahara, M. Machida, Top. Catal. 52 (2009) 2108–2111.
[25] H. Liu, L. Su, F. Liu, C. Li, U.U. Solomon, Appl. Catal. B-Environ. 106 (2011) 550–558.
[26] A. Maione, F. André, P. Ruiz, Appl. Catal. B-Environ. 75 (2007) 59–70.
[27] J.H. Zhu, Y. Wang, Y. Chun, X.S. Wang, J. Chem. Soc. Faraday Trans. 94 (1998) 1163–1169.
[28] C. Shi, P. Zhang, Appl. Catal. B-Environ. 115 (2012) 190–200.
[29] W. Xu, Z. Zhan, L. Di, X. Zhang, Catal. Today 256 (2015) 148–152.
[30] S.L. Husheer, J.G. Thompson, A. Melnitchenko, J. Solid State Chem. 147 (1999) 624–630.
[31] M. Kotwal, P. Niphadkar, S. Deshpande, V. Bokade, P. Joshi, Fuel 88 (2009) 1773–1778.
[32] W. Wang, Y. Li, X. Zhang, W. Fang, Y. Yang, Catal. Commun. 69 (2015) 104–108.
[33] X. Wen, G. Li, Q. Chen, H. Zhang, X. Ba, G. Bai, Ind. Eng. Chem. Res. 53 (2014) 11646–11652.
[34] C. Na-Chiangmai, N. Tiengchad, P. Kittisakmontree, O. Mekasuwandumrong, J. Powell, J. Panpranot, Catal. Lett. 141 (2011) 1149–1155.
[35] W. Whitmore, A. Revukas, J. Am. Chem. Soc. 62 (1940) 1687–1693.